SAMPLE POSITIONING IN NEUTRON DIFFRACTION EXPERIMENTS USING A MULTI-MATERIAL FIDUCIAL MARKER

D. Marais, A.M. Venter, J. Markgraaff, J. James

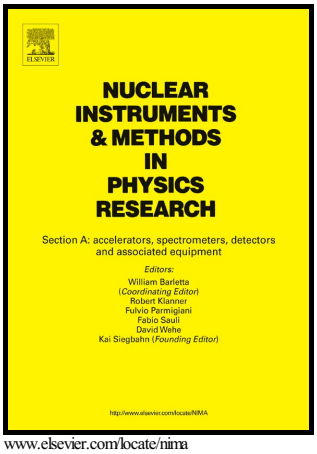

www.elsevier.com/locate/nima

PII: S0168-9002(16)31045-2
DOI: http://dx.doi.org/10.1016/j.nima.2016.10.020
Reference: NIMA59379

To appear in: *Nuclear Inst. and Methods in Physics Research, A*

Received date: 19 September 2016
Revised date: 4 October 2016
Accepted date: 10 October 2016

Cite this article as: D. Marais, A.M. Venter, J. Markgraaff and J. James, SAMPLE POSITIONING IN NEUTRON DIFFRACTION EXPERIMENTS USING A MULTI-MATERIAL FIDUCIAL MARKER, *Nuclear Inst. and Methods in Physics Research, A,* http://dx.doi.org/10.1016/j.nima.2016.10.020

SAMPLE POSITIONING IN NEUTRON DIFFRACTION EXPERIMENTS USING A MULTI-MATERIAL FIDUCIAL MARKER

D. Marais[1,2,a], A. M. Venter[1,3,b], J. Markgraaff[2,c], J. James[4,d]

[1]*Research and Development Division, South African Nuclear Energy Corporation (Necsa) SOC Limited, PO Box 582, Pretoria, 0001, South Africa*

[2]*School of Mechanical and Nuclear Engineering, North-West University, Potchefstroom, 2520, South Africa*

[3]*Faculty of Agriculture Science and Technology, North-West University, Mahikeng, 2790, South Africa*

[4]*Faculty of Mathematics, Computing and Technology, The Open University, Milton Keynes, MK76AA, England*

[a]*Corresponding author: Deon.Marais@necsa.co.za, +27123055645*

[b]*Andrew.Venter@necsa.co.za, +27 123055038*

[c]*Johan.Markgraaff@nwu.ac.za, +27 182991658*

[d]*Jon.James@open.ac.uk, +44 1908645198*

Abstract

An alternative sample positioning method is reported for use in conjunction with sample positioning and experiment planning software systems deployed on some neutron diffraction strain scanners. In this approach, the spherical fiducial markers and location trackers used with optical metrology hardware are replaced with a specifically designed multi-material fiducial marker that requires one diffraction measurement. In a blind setting, the marker position can be determined within an accuracy of ±164 μm with respect to the instrument gauge volume. The scheme is based on a pre-determined relationship that links the diffracted peak intensity to the absolute positioning of the fiducial marker with respect to the instrument gauge volume. Two methods for establishing the linking relationship are presented, respectively based on fitting multi-dimensional quadratic functions and a cross-correlation artificial neural network.

Keywords: Neutron diffraction, Strain scanning, Sample positioning, Artificial neural network

1. Introduction

1.1. Strain scanning using neutron diffraction

An inherent advantage of using neutron (and X-ray) diffraction techniques in the investigation of stresses in materials and components is the non-destructive nature of the measurements. Specific volumes are examined by the accurate positioning with respect to the instrumental gauge volume defined by the intersection of the primary and diffracted beam paths. The size and position of the respective beams are set by apertures. Internal strain caused by various inhomogeneous lattice displacement mechanisms is determined from the direct comparison of the measured diffraction peak position in the polycrystalline solid to its stress-free reference.

1.2. Traditional sample positioning

Accurate sample positioning with reference to the instrumental gauge volume is one of the most important parameters in diffraction based strain investigations. It is suggested that positional accuracy should typically be 10% of the largest dimension of the gauge volume in the diffraction plane [1]. Experience has shown that positional accuracy of about ±0.5 mm can be achieved by aligning a sample with a laser and ±0.2 mm by using theodolites. This can be further improved by performing neutron beam sample entry scans and fitting the diffracted intensity values as a function of relative position to an appropriate analytical solution [2] to give accuracies in the order of ±10 μm. The method works well for samples with a simple geometrical shape, but becomes less efficient to apply for samples exhibiting an arbitrary form which may require multiple entry scans. This becomes time-consuming with subsequent loss of the useful beam time for strain investigations.

1.3. Advanced positioning methods

To speed up the sample alignment procedure, a number of alternative positioning methods have been reported of which two are briefly introduced:

Ratel *et al.* has proposed a 'direct sample positioning and alignment methodology' where a sample of arbitrary shape is mounted on an accurately machined baseplate and sample holder [3]. The baseplate can be rapidly repositioned on the instrument within ±100 μm accuracy using locating dowels. By digitizing the sample and baseplate using a coordinate measuring machine (CMM), or laser scanner, most of the sample alignment and experiment planning can be performed off-line. A common reference point between the digitized sample plate and the physical instrument is determined by performing x, y and z entry scans on an alignment pin mounted on a separate baseplate.

Strain Scanning Simulation Software (SScanSS), developed by the Open University, UK, facilitates arbitrary sample alignment, experiment planning and measurement automation [4]. SScanSS utilizes 3D computer models of the sample and instrument in combination with spherical fiducial markers and a CMM to determine the sample's position on the instrument to within ±100 μm relative to a laboratory coordinate system.

2. Multi-material fiducial marker positioning

2.1. Considerations

Since not many neutron facilities have access to CMM's, an alternative method has been explored to determine the sample position within the SScanSS system approach. The hypothesis has been to replace the traditionally used spherical fiducial marker with a composite marker that can be directly measured with the neutron diffraction beam to determine its position. This eliminates the need of a CMM for positioning.

In order to resolve the marker position in three dimensions the following essential requirements have to be considered:

- The marker has to comprise three different materials, where each material defines a different orthogonal dimension with their intercept defining zero as a unique position;
- The materials need to render diffraction angles that are in close proximity to each other, but adequately separated, to enable their analyses from one instrument setting.

The neutron pathlength through the marker, the different scattering lengths and attenuations of the constituent materials, as well as the gauge volume filling fraction will be different for each position in the marker since the gauge volume is partially submerged in all three materials throughout. This will

lead to a distinct ratio of peak intensities with respect to the marker position. The peak intensities can therefore be used to determine the marker position relative to the gauge volume.

This approach requires a *characterization dataset* of the instrument fiducial marker combination, against which, the position of subsequent blind setups can be determined from a single diffraction detector data frame measurement.

2.2. Marker composition and geometry

The multi-material fiducial marker (MMFM) selected for this feasibility study comprised three materials specifically chosen to have Bragg peaks close to $2\theta = 90°$ at a neutron wavelength of 1.646 Å as used on the Materials Probe for Internal Strain Investigations (MPISI) instrument at the SAFARI-1 research reactor in South Africa [5]. The MMFM shown in Fig. 1 consists of a 20 x 8 x 4 mm^3 sized beryllium slab attached to a 10 x 8 x 3 mm^3 sized mild steel (ferrite; α-Fe) slab, and an 8 x 8 x 8 mm^3 sized 316L-stainless steel (austenite; γ-Fe) cube. Table 1 indicates the expected Bragg peak positions from this composite sample.

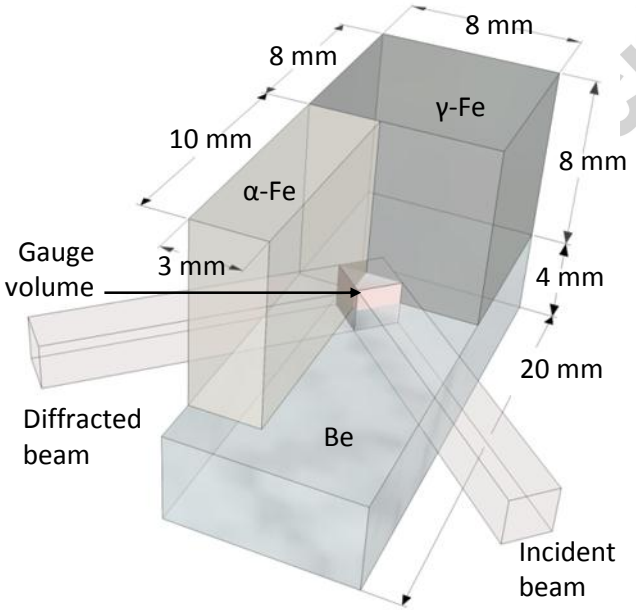

Fig. 1. Illustration showing the marker geometry and dimensions.

Table 1. MMFM diffraction peak positions when using 1.646 Å neutrons

Material	**Crystal plane**	**Diffraction angle (2θ)**
Mild steel	211	88.6º
Beryllium	110	92.1º
316L Stainless steel	311	99.6º

2.3. Experimental procedure

The MMFM was precisely constructed and set up on MPISI as shown in Fig. 2. In this configuration the beryllium and mild steel are measured in transmission geometry and the stainless steel in reflection

geometry. As the neutron pathlength remains constant through the material measured in transmission geometry, the intensity of the diffracted beam will only be a function of the filling fraction of the gauge volume. The diffracted peak intensity will systematically increase as the gauge volume moves deeper into the material and remain constant when the entire gauge volume is fully submerged in the material. In the reflection scattering geometry the neutron pathlength increases as the gauge volume moves deeper into the material. The diffracted intensity is now dependent on both the material neutron attenuation factor and the filling fraction. Subsequently, as the intercept gauge volume increases the diffracted intensity will correspondingly increase up to the position where it is fully submerged. The diffracted intensity would however also be attenuated by the depth of penetration (pathlength of the incident and diffracted beams to reach the depth of measurement). Thus the material used for the 'reflection material' should not have a large neutron attenuation since this would exacerbate this contribution.

A nominal gauge volume of 2 x 2 x 2 mm^3 was selected with the primary and secondary beam apertures positioned 20 mm from the instrument rotation axis to give good count rates and volume definition. The MPISI instrument is equipped with a 300 x 300 mm^2 position sensitive area detector at a sample-to-detector distance of 1150 mm. This gives a detector acceptance window of ~15º 2θ. By positioning the detector at 2θ = 94° the diffraction peaks from the three materials were captured simultaneously in the detector window. The zero position of the marker, required for subsequent tests, was determined from entry curves measured in the x, y and z directions. The positional accuracy was ±10 µm.

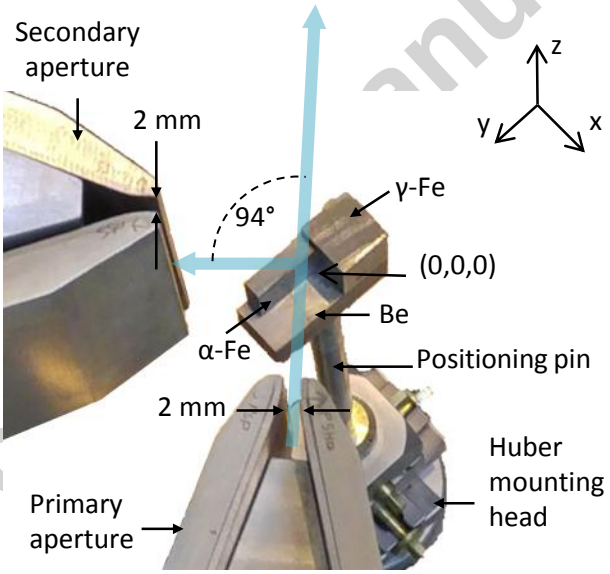

Fig. 2. Diagram showing the setup and positioning of the MMFM on MPISI.

The *characterization dataset* was acquired by sequential step-scan measurements of the MMFM through the gauge volume in all three axes directions (x,y,z) over a range from -0.5 mm to 0.5 mm with a step size of 0.17 mm and taking data for 750 s per position. This rendered 7 x 7 x 7 = 343 measurements.

A *test dataset* (to be used for testing the accuracy of the position recovery procedures) was measured by sequential step-scan measurements of the MMFM from -0.45 mm to 0.45 mm with a step size of 0.30 mm in all three axes directions through the gauge volume and taking data for 750s per position.

This rendered 4 x 4 x 4 = 64 measurements. None of these positions overlapped with the *characterization dataset*.

2.4. Data reduction

The diffraction patterns corresponding to the *characterization dataset* are shown in Fig. 3, where each measurement number corresponds to a unique x, y and z position. The diffraction data was normalized to a neutron beam monitor count rate in order to compensate for possible fluctuations in reactor power. A Gaussian peak function was fit using the in-house developed program ScanManipulator [6] to each peak to determine the peak intensity. The average relative error for the fitted intensities of the α-Fe, Be and γ-Fe peaks were 1.85%, 2.89% and 2.33% respectively. As a typical example, the diffraction pattern and fit for position (0,0,0) is shown in Fig. 4. The peak intensities as a function of position are given in Fig. 5.

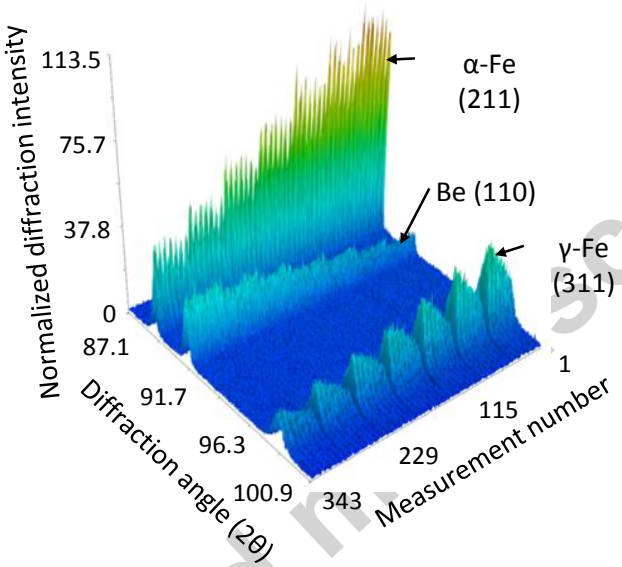

Fig. 3. Graph of the *characterization dataset* diffraction patterns

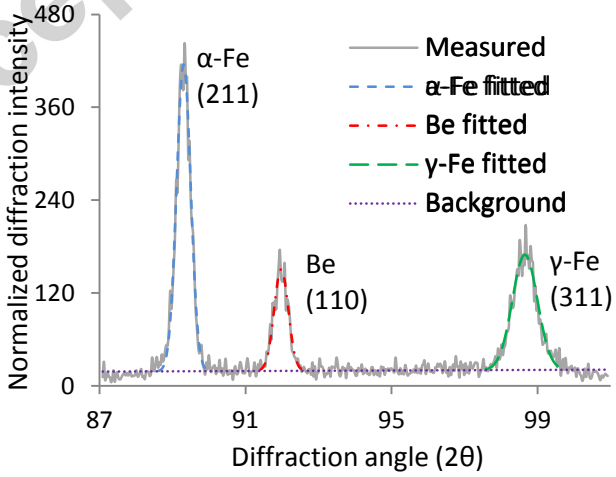

Fig. 4. Graph showing the diffraction pattern at position (0,0,0)

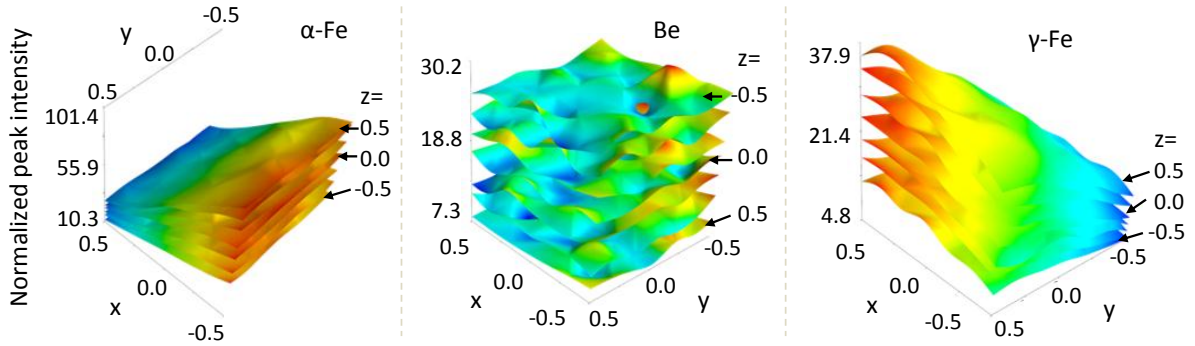

Fig. 5. Graphs showing the *characterization dataset* peak intensities as a function of position for the three materials composing the MMFM

3. Resolving the sample position from peak intensities

The technique relies on matching a measured diffraction pattern to the *characterization dataset*, to resolve the sample position with respect to the gauge volume centre. However, due to the different neutron attenuations through the different materials, the relationship between diffracted neutron intensity and marker position is non-linear. It should be noted that the intensities are also dependent on the gauge volume size and therefore a different *characterization dataset* should be established for each gauge volume size. This can be done through simulation using neutron ray-tracing software such as McStas [7], but requires a very accurate neutron optic model of the instrument. Two methods for retrieving the position were explored namely by means of multi-dimensional quadratic fitting, and by employing artificial neural network technology.

3.1. Multi-dimensional quadratic fitting

Visual inspection of the graphs presented in Fig. 5, indicates that each of the x, y and z surfaces can be approximated by a quadratic function. The normalized peak intensity (I) for each material with respect to position can be approximated by an equation of the form:

$$I_{material}(x,y,z) = (a_x x^2 + b_x x + c_x)(a_y y^2 + b_y y + c_y)(a_z z^2 + b_z z + c_z) \qquad \text{Eq. 1}$$

with a_x, b_x, c_x, a_y, b_y, c_y, a_z, b_z, and c_z constants determined using a least-squares method. Fig. 6 shows the fitted multi-dimensional quadratic functions of the *characterization dataset*.

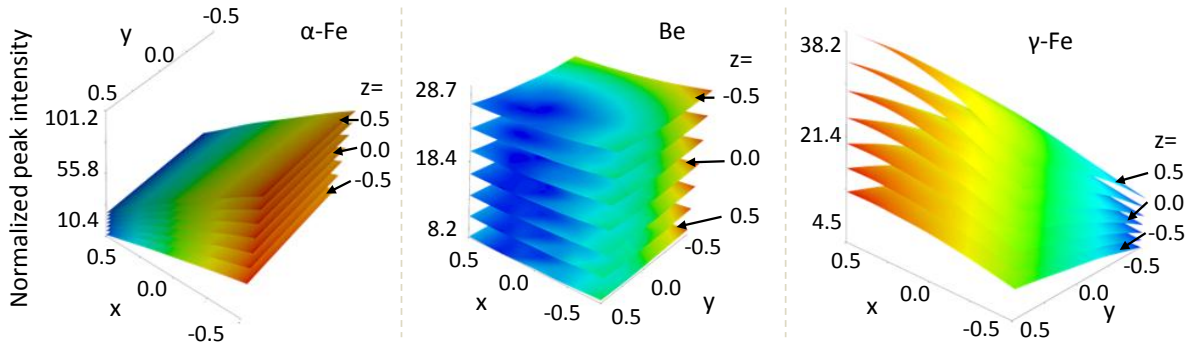

Fig. 6. Graphs showing the peak intensities as a function of position determined from a least-squares multi-dimensional quadratic function fit to the *characterization dataset.*

This enables determination of the marker position from an iterative analysis using a least-squares method. As a starting point, an initial marker position where x = y = z = 0 is assumed. The measured normalized peak intensity of Be is then used to refine the marker's z-position as it is mostly insensitive to the x and y positions. Next x is refined from the α-Fe equations, followed by y from the γ-Fe equations using the most recent position values at each step. The process is repeated until convergence is reached.

3.2. Cascade-correlation artificial neural network

Artificial neural networks (ANN) have been used in various disciplines to establish complex non-linear relationships between input and output datasets. An ANN consist of a number of interconnected nodes (neurons), arranged in one or more hidden layers, which propagates a signal to other neurons based on the strength of the incoming signals [7]. A neuron is defined by an activation function such as the sigmoid given in Eq. 2, or some other non-linear 'step-like' function.

$$y_j = \frac{1}{1 + e^{-x_j}} \qquad \text{Eq. 2}$$

where y_i is the neuron output and $x_j = \sum_i y_i w_{ji}$ is the sum of all the weighted input signals. The weights (w_{ji}) connecting the neurons are adjusted, or trained, in some way (for instance by employing the back-propagation algorithm [9]) in order to represent the system defined by an input-output dataset.

The cascade-correlation algorithm automatically creates a multi-layer ANN by training a candidate hidden layer through fixing the weights of its inputs and inserting in the network after an acceptable error has been reached [10]. It is also possible to perform this training on multiple candidates in parallel and selecting the best solution based on a correlation function. After installation, should the error be unacceptable, the network is re-evaluated on the entire dataset and another candidate hidden layer created. A diagram of a two-input, two-output, two hidden layer cascade-correlation ANN is shown in Fig. 7.

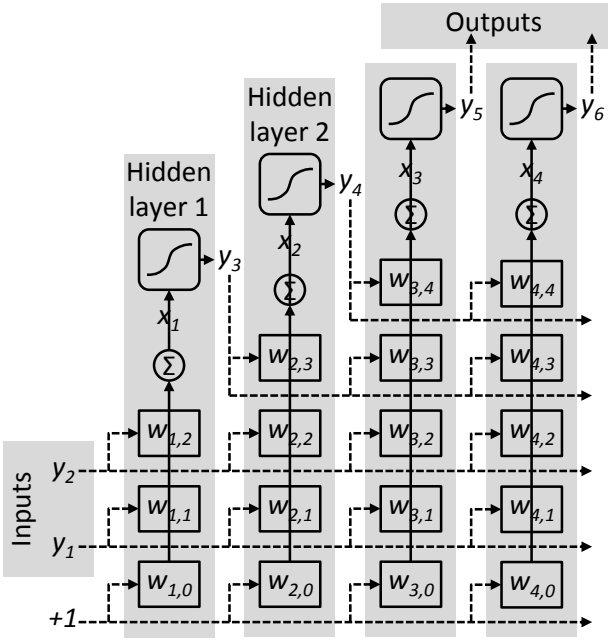

Fig. 7. Diagram of a cascade architecture ANN after two hidden layers were added.

The Fast Artificial Neural Network (FANN) library [11] was used to train a 5 hidden layer cascade-correlation ANN using the peak intensities as inputs and the x, y and z positions as outputs.

4. Method evaluation

The normalized peak intensities for the *test set* were calculated in the same manner as the *characterization dataset*. Each position of the *test set* was evaluated using the multi-dimensional quadratic fitting method as well as the cascade-correlation ANN. The calculated positions were compared with the real positions to estimate the accuracy of the different methods. The x, y and z positional errors for the two methods are shown in Fig. 8 and Fig. 9 respectively.

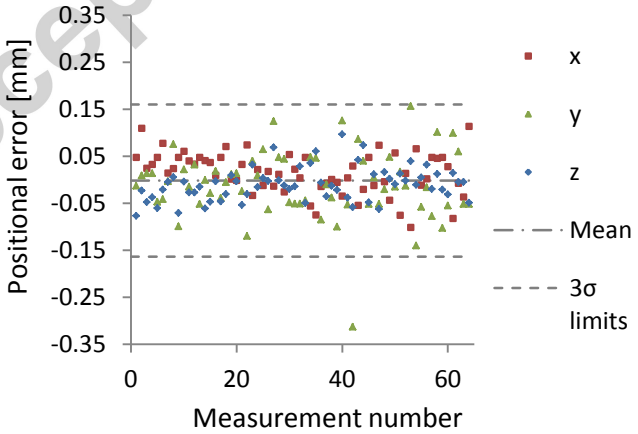

Fig. 8. Scatter plot showing the positional errors for the *test set* evaluated using the fit quadratic functions.

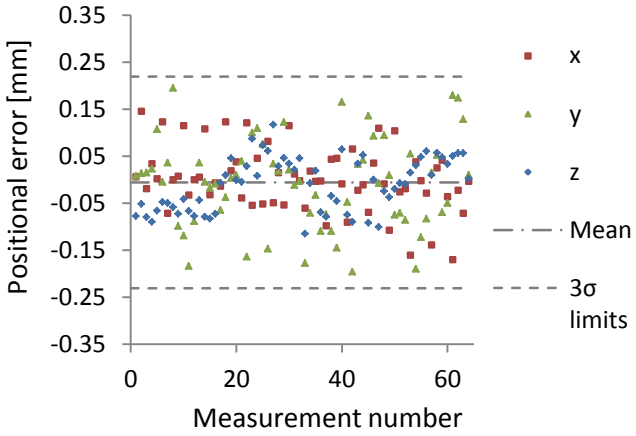

Fig. 9. Scatter plot showing the positional errors for the *test set* evaluated using the ANN approach.

The 3σ confidence level for the fit quadratic function approach is ±164 µm and that of the ANN is ±231 µm. The dataset of the ANN however shows that the all the data points were within the ±200 µm acceptable error range.

Conclusion

Both methods (multi-dimensional quadratic fitting and cascade-correlation artificial neural network approach) can be used to determine the marker position using a single detector data frame. The fit quadratic function approach is computationally more intensive than the ANN, as the position is recovered through an iterative approach. This can however be automated. Retrieving the position from a successfully trained ANN is trivial and experiments have shown that all recovered positions were within an acceptable error range. In a blind setting, accurate positioning can thus be done with one measurement to accuracy of ±164 µm when using a 2 x 2 x 2 mm^3 gauge volume.

Acknowledgements

This research is supported by the National Research Foundation of South Africa, grant number 84234, and Necsa SOC Limited. Any opinion, finding and conclusion or recommendation expressed in this material is that of the author(s) and the NRF does not accept any liability in this regard.

References

[1] G.A .Webster, R.W. Wimpory (Eds.), Polycrystalline materials determination of residual stresses by neutron diffraction, ISO/TTA3, Geneva, (2002).
[2] P.C. Brand, H.J. Prask, J. Appl. Cryst. 27 (1994) 164-176.
[3] N. Ratel, D.J. Hughes, A. King, B. Malard, Z. Chen, P. Busby, P.J. Webster, Rev. Sci. Instrum. 76 055103(2005)
[4] J.A. James, J.R. Santisteban, L. Edwards, M.R. Daymond, Physica B, 350 (2004) 743-746
[5] Necsa SOC Limited, MPISI - Materials Probe for Internal Strain Investigations, http://www.necsa.co.za/Products-and-Services/Research/Facility-and-Instrument-characteristics/MPISI, Date of access: 30 August 2016

[6] D. Marais, A.M. Venter, J. Markgraaff, Data processing at The South African Nuclear Energy Corporation SOC Ltd (Necsa) neutron diffraction facility, Proceedings of SAIP2015, (2016) 198-203.

[7] P. Willendrup, E. Farhi, K. Lefmann, Physica B, 350 (2004) 735.

[8] R. Rojas, Neural Networks – A Systematic Introduction, Springer-verlag, Berlin, 1996

[9] D.E. Rumelhart, G.E. Hinton, R.J. Williams, Learning presentations by back-propagation errors, Nature, 323 (1986) 533-536

[10] S.E. Fahlman, Lebiere C. in: D.S. Touretzky (Ed.), Advances in neural information processing systems 2, Morgan Kaufman Publishers Inc, San Francisco, (1990) 524-532

[11] S. Nissen, Implementation of a Fast Artificial Neural Network Library (FANN-2.1.0). Report, Department of Computer Science University of Copenhagen (DIKU), 31(2003) https://sourceforge.net/projects/fann/. Access date: 2015/07/22